# Adsorption of semiflexible polymers in cylindrical tubes

A. Milchev[1*], K. Binder[2]
[1] *Institute of Physical Chemistry, Bulgarian Academy of Sciences, 1113 Sofia, Bulgaria [milchev@ipc.bas.bg] and*
[2] *Institut für Physik, Johannes Gutenberg-Universität Mainz,*
*Staudinger Weg 9, D-55099 Mainz, Germany [kurt.binder@uni-mainz.de]*

**Abstract**

Conformations of wormlike chains in cylindrical pores with attractive walls are explored for varying pore radius and strength of the attractive wall potential by Molecular Dynamics simulations of a coarse-grained model. Local quantities such as the fraction of monomeric units bound to the surface and the bond orientational order parameter as well as the radial density distribution are studied and the global chain extensions parallel to the cylinder axis and perpendicular to the cylinder surface. A nonmonotonic convergence of these properties to their counterparts for adsorption on a planar substrate is observed due to the conflict between pore surface curvature and chain stiffness. Also the interpretation of partially adsorbed chains in terms of trains, loops and tails is discussed.

## I. INTRODUCTION

Understanding the behavior of polymers in cylindrical confinement is a longstanding challenge[1–47] and relevant for a broad variety of applications, e.g., oil recovery from porous rocks[48–50], single molecule sensing[51] and DNA translocation[52,53] through artificially produced channels[54–56], and other microfluidic or nanofluidic devices[54,55]. Also in biology the transport of biopolymers in biologically formed channels plays a role.

The theoretical studies of this problem[3–7,9,10,14,16–47], have focused almost exclusively on the confinement in pores and nanochannels with repulsive surfaces (typically modeled by rigid hard walls). However, the question of how a long flexible or semiflexible polymer can enter into such a cylindrical pore (or nanochannel with square or rectangular cross section) is a nontrivial problem: a flexible macromolecule with linear chemical architecture and $N$ monomeric units in dilute solution has a typical radius $R_e = \ell_b\sqrt{N}$ in Theta-solvents and $R_e = \ell_b N^\nu$ with $\nu = 3/5$ under good solvent conditions[57], $\ell_b$ being the bond length between subsequent monomeric units along the chain. However, a flexible polymer in a narrow tube of diameter $D$ has a linear dimension along the tube of order $R_z = N\ell_b^2/D \gg R_e$ for Theta conditions[9] and $R_z = ND(\ell_b/D)^{1/\nu}$ under good solvent conditions[3] (prefactors of order unity here are suppressed throughout). The situation is even more extreme for long semiflexible polymers with persistence length[58–60] $\ell_p \gg \ell_b$, which have a radius[61] $R_e = (\ell_p\ell_b N)^{1/2}$ for contour lengths $L = N\ell_b$ less than $L^* = \ell_p^3/\ell_b^2$ where under good solvent conditions excluded volume effects set in[62–64]: For $D \ll \ell_p \ll L$ one finds $R_z$ to be almost equal to $L$[14,35], if one is in the regime where hairpins[25,29] are not yet important[37,42,44,45]. This large discrepancy between $R_z$ and $D$ has the consequence that the partition coefficient[1,2,8,10,12,13,15], defined as the fraction of chains in the pore relative to the fraction of chains in the dilute solution which is in equilibrium with the chains in the pore, is extremely small. This partition coefficient $K$ is related to the free energy difference $\delta F$ between the confined and unconfined chains via $K = \exp(-\delta F/(k_BT))$, and for semiflexible chains in the limit $D \ll \ell_p \ll L$ one also finds[4,35] that $\delta F/(k_BT) \propto (L/\ell_p)(\ell_p/D)^{2/3}$, while for a flexible polymer[3,16] $\delta F/(k_BT) \propto R_z/D$.

The smallness of the partition coefficient is a clear hindrance for applications such as separation processes for filtration, size-exclusion chromatography, etc. A recipe to overcome this is to exploit adsorption compensation of this free energy cost using liquid chromatography near the critical adsorption conditions[65–69], and this has motivated theoretical studies for flexible polymers[18]. While the adsorption transition of flexible chains on planar surfaces has been studied extensively since a very long time (e.g.,[70–73]), the adsorption transition of semiflexible polymers on planar surfaces

has only been clarified much more recently[74–79]. In both cases, an interesting singular behavior is predicted in the limit $N \to \infty$. Considering the adsorption of a long macromolecule on the surface of a cylindrical pore, one can expect a rounding of this phase transition, and this finite size effect[80] becomes the more pronounced the smaller the diameter $D$ of the pore. This modification of the character of the adsorption transition should be particularly pronounced for semiflexible polymers, since the persistence length $\ell_p$ can be a mesoscopic length (e.g., $\ell_p = 50\ nm$ for ds-DNA[33]), i.e., of the same order as the tube diameter. Adsorbing a persistent segment on the inner wall of the tube is much easier when the segment is oriented parallel to the tube axis rather than perpendicular to it. Thus, the adsorption behavior can be expected to be rather different from its counterpart of a planar surface.

Often it is assumed that the choice of purely repulsive pore walls is appropriate due to electrostatic effects[33] but it is also known that under many circumstances attractive interactions between a polymer and a surface operate, e.g., van der Waals forces or screened electrostatic forces[81], e.g., DNA, may adsorb on mica[82] or on bilayer membranes[83], etc. Also neutral synthetic polymers are typically adsorbed in pores due to van der Waals forces, as capillary rise experiments with alkanes such as $C_{24}H_{50}$ in Vycor pores suggest[84]. These examples are clear enough to show that adsorption of polymers in cylindrical pores is of widespread interest.

Note that in this paper we do not at all consider electrostatic interactions explicitly (if they are present, it is assumed they are strongly screened). The problem of electrostatic interactions and their effect on adsorption of polyelectrolytes in confined geometries has been comprehensively discussed recently by de Cavalho et al.[85]

In this paper we shall fill this gap in the understanding of polymer adsorption on curved substrates by Molecular Dynamics simulations of a coarse grained model, which is described in Sec. II, extending our previous work on adsorption of semiflexible polymers on planar surfaces[77–79]. Sec. III presents our numerical results and interprets them tentatively in terms of the pertinent theoretical concepts, emphasizing the change of polymer conformations due to the curvature of the adsorbing wall in comparison with a planar adsorbing surface with the same adsorption potential. Finally Sec. IV gives a short summary and presents an outlook to further work.

## II. MATERIALS AND METHODS

We follow our previous work[77–79,86] by describing semiflexible polymers in terms of a bead - spring model with a purely repulsive Weeks-Chandler-Andersen[87] (WCA) type potential between any pair of beads at distance $r$,

$$U_{\rm WCA}(r) = \begin{cases} 4\varepsilon \left[ \left(\frac{\sigma}{r}\right)^{12} - \left(\frac{\sigma}{r}\right)^{6} \right] + \varepsilon, & r \le 2^{1/6}\sigma \\ 0, & r > 2^{1/6}\sigma \end{cases} , \tag{1}$$

choosing the potential strength $\epsilon = 1$, putting the thermal energy $k_B T$ to unity as well, and the range $\sigma = 1$ serves as the length unit. This interaction ensures the presence of excluded volume interactions, appropriate for very good solvent conditions. Successive monomers along the chain experience also the finitely extensible nonlinear elastic (FENE) potential[88]

$$U_{\rm FENE}(r) = \begin{cases} -\frac{kr_0^2}{2} \ln\left(1 - \frac{r^2}{r_0^2}\right), & r < r_0 \\ \infty, & r \ge r_0 \end{cases} . \tag{2}$$

The constants are chosen as $r_0 = 1.5\sigma, k = 30\epsilon/\sigma^2$, as previously. Note that Eqs.(1,2) together create a potential for the bond length with a sharp minimum at $\ell_b = 0.97\sigma$. Eqs.(1,2) constitute a standard

model for flexible polymers[89] and can be extended to semiflexible polymers by supplementing it with a bond angle potential

$$U_{\rm bend}(\theta_{ijk}) = \epsilon_b[1 - \cos(\theta_{ijk})] \tag{3}$$

where $\theta_{ijk}$ is the bond angle formed between the two subsequent unit vectors along the bonds connecting monomers $i$ with $j$, and $j$ with $k$, respectively, when we label monomeric units along the chain molecule from $i = 1$ to $i = N$. For large stiffness $\kappa = \epsilon_b/(k_BT)$ Eqs.(1-3) can be considered as a generalized discretized version of the Kratky-Porod[61] model, but including excluded volume. We would obtain precisely the continuum version of the original Kratky-Porod (KP) model in the limit $N \to \infty$, contour length $L = (N-1)\ell_b$ being held fixed, and hence both $\ell_b \to 0, \sigma \to 0$. In this limit, the persistence length $\ell_p$ gets a precise meaning in terms of the correlation function $C(s-s')$ between tangent vectors to the space curve $\vec{r}(s)$ describing the polymer contour, $s$ is a coordinate running along the contour. One has

$$C(s-s') = \langle \cos(\theta(s-s'))\rangle = \exp(-(s-s')/\ell_p) \tag{4}$$

and $\ell_p$ there is related to $\kappa$ via

$$\ell_p = \kappa \ (d=3); \quad \ell_p = 2\kappa \ (d=2). \tag{5}$$

Since in $d = 3$ dimensions the chain can bend locally in two directions away from the tangent vector, but only in one direction in $d = 2$, the persistence length in $d = 2$ is twice as large as in $d = 3$, according to the KP-model.

Now it is well known that in the presence of excluded volume, for the limit $N \to \infty$, the exponential decay of Eq.(4) fails for large enough distance $s - s'$, and is replaced by a power law[60,62–64,90]. For chains adsorbed on planar surfaces, an even more complicated behavior has been found[77–79]. For distances of the order of a few bond lengths, $C(s)$ for a stiff chain has a decay compatible with $C(s) = \exp(-s/\ell_{p,eff})$ where $\ell_{p,eff}$ is essentially the $d = 3$ persistence length. For larger $s$ then a gradual crossover occurs to $C(s) = A\exp(-s/\ell_{p,eff})$ with an amplitude $A$ slightly smaller than unity, while $\ell_{p,eff}$ then takes a value close to the $d = 2$ value of $\ell_p$ in Eq.(5). However, for distances $s$ of the order of $\ell_{p,eff}$ itself, a crossover to the asymptotic power law[90] $C(s) \propto 1/\sqrt{s}$ starts to set in[77–79]. In the present work we shall not study how this behavior is modified when adsorption on a cylindrical surface takes place: the cylindrical confinement causes a slight nonzero average of bond vector orientations along the $z$-axis, and hence an even more complicated behavior must arise. Thus, we consider only the short-distance estimate describing the initial decay of bond-orientational correlations, defined via[86]

$$\ell_{p,eff}/\ell_b = -1/(\ln\langle\cos(\theta_{ijk})\rangle). \tag{6}$$

As an example, Fig.1 shows a plot of this effective persistence length versus the strength of the adsorption potential, which will be specified below, for various choices of the tube radius $R$. For nonadsorbed polymers with $\kappa = 25$ one has[77–79] $\ell_{p,eff} = 24.3$ in dilute solution in $d = 3$; note that $\ell_b = 0.97\sigma$ and hence one indeed expects $\ell_p = \kappa\ell_b = 24.25$. We see from Fig.1 that for nonadsorbed chains (for the present model the adsorption transition on a planar surface has been estimated to occur for[77–79] $\epsilon_a^{cr} = 0.48(1)$ for $\kappa = 25$) $\ell_{p,eff}$ does not depend on $\epsilon_a/(k_BT)$, as expected, since the confined chains then are rarely near the surface, and hence insensitive to the adsorption potential. However, there is a clear increase with decreasing radius $R$ (i.e., increasing confinement) up to about 3% for $R = 8\sigma$. In contrast, in the adsorbed phase, there is a clear increase with increasing $\epsilon_a/(k_BT)$,

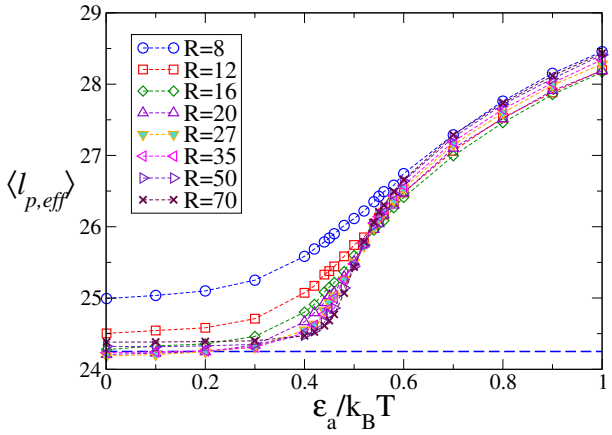


FIG. 1. Variation of the persistence length $\ell_{p,eff}$ defined from Eq.(6) with adsorption strength $\epsilon_a$ for tubes with radius $R$ as indicated. Here $N = 200$, $\kappa = 25$, and $\ell_p = 24.25$, shown as broken horizontal line.

up to the order of 15% in the shown regime! This is still far below the theoretical $d = 2$ value, and hence the data in Fig.1 show that Eq.(5) is not really useful to interpret the actual behavior of the confined chains for small distances along the chain.

As a consequence, we conclude that the stiffness $\kappa$, defined in terms of an interaction parameter $\epsilon_b$ of the model Hamiltonian, Eq.(4), is a well-defined property, while the "persistence length" is not at all a unique property of a given type of polymer since it depends on global conditions of the environment in which the polymer exists such as a wide tube with attractive walls.

Also the pore wall is described in our model in a coarse-grained fashion only, assuming a structureless perfectly rigid cylindrical surface, at which a potential acts that depends only on the radial distance $r' = R - r$ (we choose the origin of the coordinate system on the cylinder axis)

$$U_a(r') = \epsilon_a C \Big[ \Big( \frac{\sigma_w}{r'} \Big)^{10} - \Big( \frac{\sigma_w}{r'} \Big)^{4} \Big] \quad . \tag{7}$$

where the constant $C = \frac{5}{3} \left(\frac{5}{2}\right)^{2/3}$ so that the minimum at $r'_{min} = \left(\frac{5}{2}\right)^{1/6}$ has the depth $-\epsilon_a$, For simplicity, the range parameter $\sigma_w$ is chosen equal to $\sigma$, hence $\sigma_w = 1$. We do not consider any explicit dependence of this potential on $R$, which would result if the potential is constructed by summing over the pairwise Lennard-Jones (LJ) interactions between a considered pointlike particle and all the atoms located in the cylindrical surface plane.

Note that often a Mie-potential with $(9, 3)$ powers rather than $(10, 4)$ is chosen instead of Eq.(7) to describe the coarse-grained particle-surface interaction. The $(9, 3)$ powers arise when the LJ interactions are summed over all atoms in a three-dimensional halfspace rather than only its $d = 2$ surface. However, experiments show that often the actual surface potential is due to $d = 2$ surfactant layers, e.g., the wetting properties of water on silicon surfaces can be varied all the way from complete drying (repulsive water - $Si$-forces) to complete wetting (attractive water - $Si$-forces) when the $Si$ surface is appropriately coated[91]. In view of the complicated physical chemistry of the DNA- surface interactions (see, e.g.,[82] and references therein) it may seem questionable whether the model studied here is qualitatively applicable to real systems of experimental interest. However, in the context of translocation experiments of DNA and RNA through long nanopores[92] it has been shown that a model very similar to the present one reproduces the experimental trends strikingly well. While in such studies the length of the (open) pore is an important parameter, here we use a cylinder of height $H = 200\sigma$ (i.e., longer than the contour length $L = (N - 1)\ell_b$ where we use $N = 200$) with

periodic boundary conditions in $z$-direction, representing hence a pore of almost macroscopic length, where pore end effects are negligible.

The pore radii are in the range from $R = 8\sigma$ to $R = 70\sigma$ throughout; the latter choice is already of the order of the end-to-end distance for $N = 200$, as one can see from the estimate from the Kratky Porod model.

The MD methods applied here are standard and have been described in detail previously[47,79]. Again we use the recipe to run $\mathcal{N} = 50$ chains in parallel in the same volume;, Fig.2. These chains do not interact with each other yet this allows a straightforward parallelization using the HOOMD - Blue software on graphics processing units (GPU's)[93,94]. The MD time step was chosen $\delta = 0.005\tau_{MD}$ where $\tau_{MD} = \sqrt{(m\sigma^2/\epsilon)}$ when we choose the monomer mass $m = 1$ as well. The length of the MD runs was typically $10^7$ such time units. The starting configuration of the chain is taken as a straight

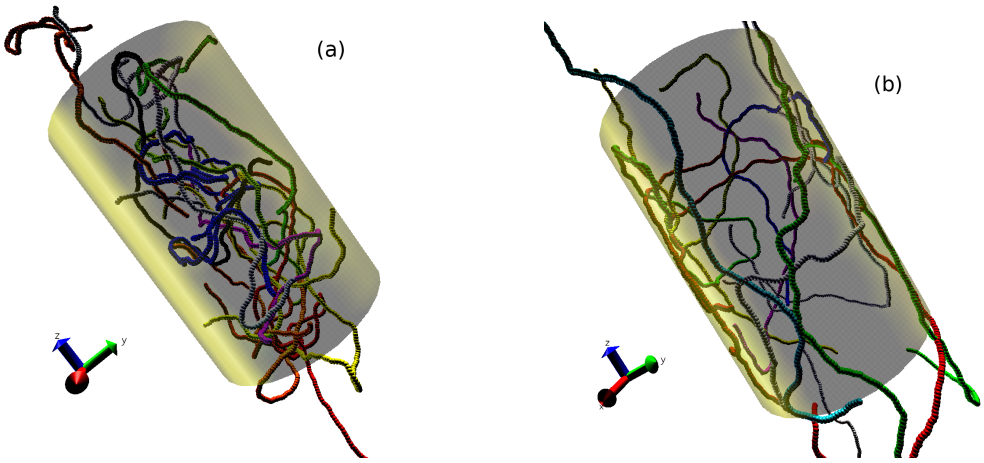


FIG. 2. Snapshots of single (noninteracting with one another) semiflexible chains in a tube with radius $R = 35$: (a) For $\epsilon_a = 0.10$ (desorbed), and (b) $\epsilon_a = 0.70$ (adsorbed). Chain integrity is preserved given the PBC along the $z$-axis. Note that we have $\mathcal{N}$ separate systems, containing just a single chain each, whereby 15 were superposed in these snapshots.

rod along the cylinder axis whereby the system was run initially for $10^6$ time units before before starting a production run.

## III. RESULTS AND DISCUSSION

### A. Local order parameters

A quantity that is straightforward to record is the radial density profile $\rho(r)$ of the monomer density, Fig.3. It is seen that for $\epsilon_a$ much less than the critical value $\epsilon_a^{cr}$, where the adsorption transition takes place at a planar wall, $\epsilon_a^{cr} = 0.48(1)$[77–79], $\rho(r)$ has a flat maximum at the cylinder center. Near $r = 0.75R$, $\rho(r)$ has decreased to about $\rho(0)/2$, and only in the regime from $r' = R - r = 2$ and closer to the surface, the density decays rapidly to zero as a consequence of the repulsive part of the potential. However, at about $\epsilon_a \approx 0.4$ the curvature of $\rho(r)$ at $r = 0$ changes sign, and for $\epsilon_a = 0.5$ and larger at the cylinder axis a density minimum occurs while a density maximum is then found in the regime $1 < r < 2$, due to monomers adsorbed at the cylinder surface. The height of this peak increases smoothly with $\epsilon_a$ but clearly the peak becomes the sharper the larger $R$ is. Of course, a well-defined sharp adsorption transition, as it occurs for $N \to \infty$ at a planar surface, cannot take place at the cylindrical surface: the finite size of $R$ causes a rounding of the singularities that occur for $\epsilon_a^{cr}$ at the planar surface. As we shall see, the simulation results obtained here suggest that

the finite size effects due to the smallness of $R$ are still more important than the finite size effects associated with the finite value of $N$ ($N = 200$ here throughout).

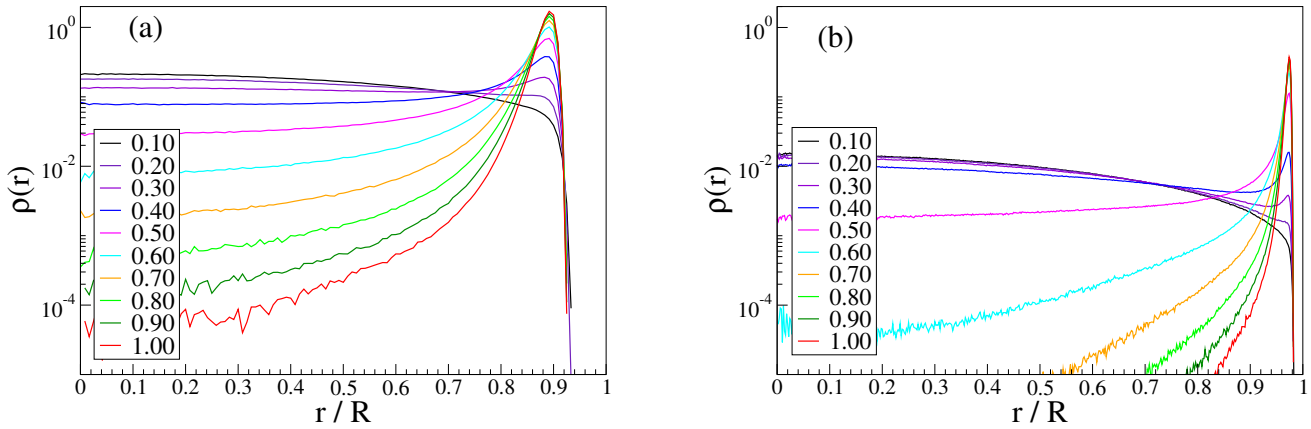


FIG. 3. Radial density distribution $\rho(r)$ of a semiflexible polymer in a tube of radius $R = 12$ (a) and $R = 50$ (b). Several distinct choices of $\epsilon_a$ (in units of $k_BT$) are indicated. The normalization integral $\int_0^R \rho(r) r dr = 1$ has been chosen (with $\sigma = \sigma_w = 1$ as the unit of length throughout).

To precisely define the fraction of adsorbed monomers $f$ we have previously suggested to weight the density with the adsorption potential[77–79], which would mean in our case

$$f = \int_{\sigma_w}^{R} dr'(R - r')U_a(r')\rho(r') / \int_{\sigma_w}^{R} dr'(R - r')U_a(r') \tag{8}$$

Note that in[77–79] due to a typo the lower integration limit of the integral was zero, but the integration must be extended only over the range where the potential is attractive, of course. Yet Eq.(8) is less useful when we want to distinguish in an individual chain configuration whether a monomer is "adsorbed" (then we say it belongs to a "train") or not (then the monomer belongs to a "loop" or a "tail", see Refs.[77–79]). Thus in practice we have opted for the simple procedure to count a monomer as "adsorbed", if its distance from the surface is within the range $r' < 2$, and non-adsorbed else. Then in any configurations $f = N_a/N$ where $N_a$ is the total number of adsorbed monomers in this configuration. Although the choice of this cutoff $r' = 2$ is somewhat arbitrary, the results for $f$ are hardly distinct from the results one would get from Eq.(8).

Fig.4a shows a plot of $f$ vs. $\epsilon_a$ for all the choices of the cylinder radius $R$ that were studied. It is seen that even when $\epsilon_a = 0$ there is still a nonzero fraction of monomers which is then counted as adsorbed; this is a finite size effect associated with the finite manitude of $R$. We find that $f$ decreases rapidly with increasing $R$ in the nonadsorbed regime, namely $f \propto 1/R^2$ (see Fig. 4b) while near $\epsilon_a^{cr}$ the decay is much slower. We estimate $f_{cr} \propto 1/R^{\zeta}$ with an exponent $\zeta \approx 0.3$. The imprecise knowledge of $\epsilon_a^{cr}$ precludes us from quoting a precise value for this exponent. For $\epsilon_a > \epsilon_a^{cr}$ the data converge rather fast to nonzero values of $f$, which are close to unity (meaning that all monomers belong to a single "adsorbed "train"). For the orientational order parameter defined below in Eqs.(10),(11) we find a similar behavior although the asymptotic region seems to be reached for the choices of $R > 20$ only.

The rapid decay of $f$ with $R$ in the nonadsorbed regime is simply understood from the fact that the density of Gaussian chains near a repulsive walls in a confined geometry scales proportional to $(r'/R)^2$. For $\kappa = 25$, $N = 200$ in three dimensions excluded volume effects are still negligible, therefore Gaussian chain statistics applies. An interesting issue is also the variation of the location $\epsilon_a^{infl}$ of the inflection point of the curves $f$ vs. $\epsilon_a$ with $R$ as well as the value $f_{infl}$ of $f$ at the inflection point itself (Fig.4c). Very roughly, we find $\epsilon_a^{cr} - \epsilon_a^{infl} \propto 1/R$ (Fig.4c) and $f_{infl} \propto 1/R^{\zeta}$.

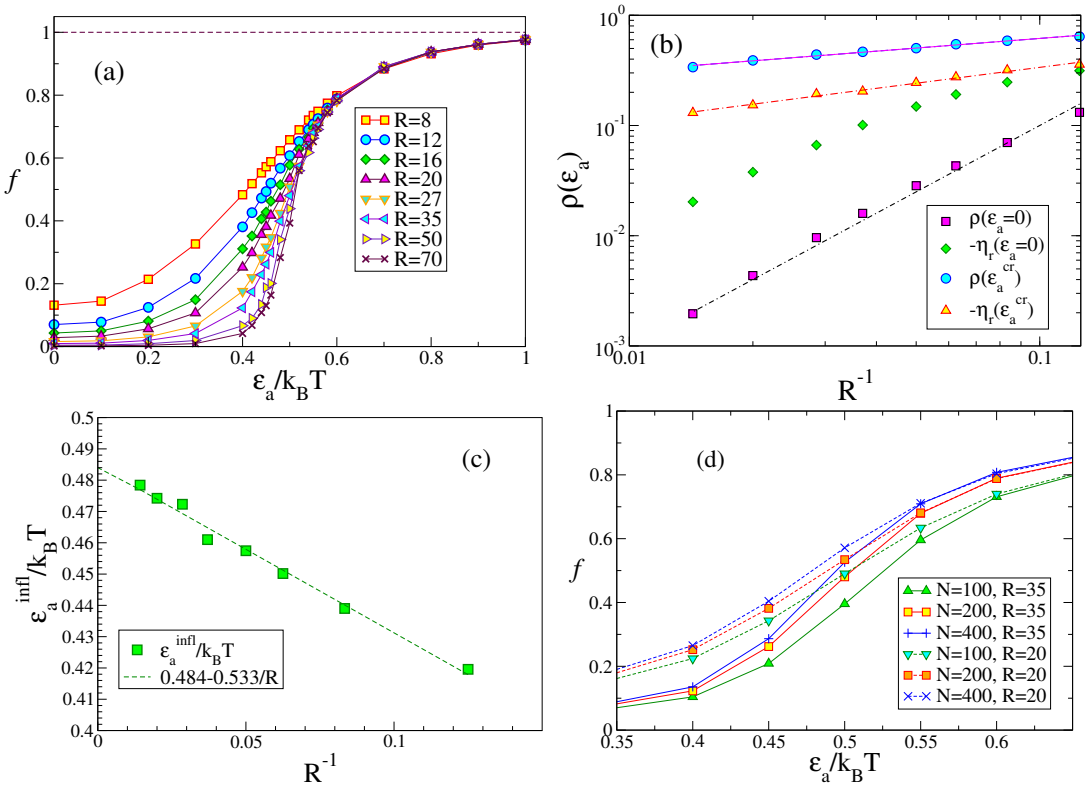


FIG. 4. (a) Adsorbed fraction $f$ of monomers plotted as function of the wall potential strength, using $N = 200$ and $\kappa = 25$ throughout, for cylinder radii from $R = 8$ to $R = 70$, as indicated. Curves are guides to the eye only. (b) Log-log plot of $f$ vs. $R$ for $\epsilon_a = 0$ and $\epsilon_a^{cr} = 0.48$, as indicated, taken from the data in panel (a). We have also included corresponding data for the orientational order parameter defined below in Eqs.(10),(11). The straight lines through the critical values indicate effective exponents $-0.29 \pm 0.01$ and $-0.48 \pm 0.02$, respectively. (c) Plot of $\epsilon_a^{infl}$ vs. $1/R$. (d) Adsorbed fraction $f$ plotted vs. $\epsilon_a$ using $N = 100$, 200 and 400, for two choices of $R$, namely $R = 20$ and $R = 35$.

In Fig.4d we address the claim made above that it is the finite size of the tube radius $R$ and not the finite size of the contour length $L = (N-1)\ell_b$ that controls the rounding of the adsorption transition which we can see in Fig.4a. Comparing the data for $f$ for $N = 100$, 200 and 400 for two typical choices of $R$ we see that $N = 100$ is clearly somewhat too short while the difference between the results for $N = 200$ and $N = 400$ exceeds the magnitude of our symbols (which is representative of our statistical errors) only slightly. Of course, for $R \gg \ell_p$ we expect that the rounding will be controlled more and more by the finite size of $N$, as it is the case for planar surfaces[77–79].

Other interesting local order parameters concern the orientation of bond vectors. Since there are two special directions associated with cylindrical confinement, one being the $z$-direction along the cylinder axis, the other the radial direction from the axis to the cylinder surface, we monitor the average orientation of a bond vector relative to these axes in terms of the parameters $\bar{\eta}_z$ and $\bar{\eta}_r$, respectively. The overbars are used to indicate that both order parameters can also be estimated spatially resolved as functions of the distance $r$ between the mid-point of the bond vector and the cylinder axis, Fig.5a. These order parameters are defined as

$$\eta_z(r) = (3\langle\cos^2(\vartheta(r))\rangle - 1)/2, \tag{9}$$

$\vartheta(r)$ being the angle between the bond vector and the $z$-direction, and

$$\eta_r(r) = (3\langle\cos^2(\alpha(r))\rangle - 1)/2, \tag{10}$$

$\alpha(r)$ being the angle between the bond vector and the radial direction, while the averages are defined

as

$$\bar{\eta}_z = \int_0^R \rho(r)\eta_z(r)rdr,\ \bar{\eta}_r = \int_0^R \rho(r)\eta_r(r)rdr \tag{11}$$

using a normalization $\int_0^R \rho(r)rdr = 1$. The order parameter $\eta_z(r)$ is positive for nonadsorbed chains and bends towards unity for $r \to R$ as stiff chains very close to the cylindrical surface are predominantly aligned in $z$-direction as well as since then there is no conflict between chain stiffness and the curvature of the cylinder surface. The radial component $\eta_r(r)$ for not so large $R$ is predominantly negative, given that bond vectors are rarely parallel to the radius vector. Interestingly, for $\epsilon_a > \epsilon_a^{cr}$ one observes a different behavior: only very few chains form large loops leading away from the surface and then entries occur where $\eta_z(r)$ can be negative, and $\eta_r(r)$ can be positive, Fig.5a. Due to the smallness of $\rho(r)$ in this regime, however, this unexpected behavior has a negligible effect on the behavior of the averages, see, e.g., Fig.5b: we see that $\bar{\eta}_r$ is always on average negative, and rather close to the limiting behavior $\bar{\eta}_r = -1/2$ for bonds that are perfectly perpendicular to the radius vector, as expected for bonds strongly adsorbed on the cylindrical surface. In the nonadsorbed regime, however, we obtain again that $\bar{\eta}_r \to 0$ with increasing $R$, compatible for large $R$ with a relation $\bar{\eta}_r \propto 1/R^2$, as in the case of $f$ (Fig.4b). Interestingly, at $\epsilon_a^{cr}$ (which almost coincides with the inflection points of the curves $\bar{\eta}_r$ vs. $\epsilon_a$) we have a decay $\bar{\eta}_r \to 0$, compatible with a similar power law as $f_{cr}$ (Fig.4b). While the apparent exponent for the power law of $f_{cr}$ is $-0.29 \pm 0.01$, for $\eta_{r,cr}$ it is $-0.48 \pm 0.02$. Clarifying whether these effective exponents are the true asymptotic exponents, and interpreting these values theoretically is a challenge that must be left for the future.

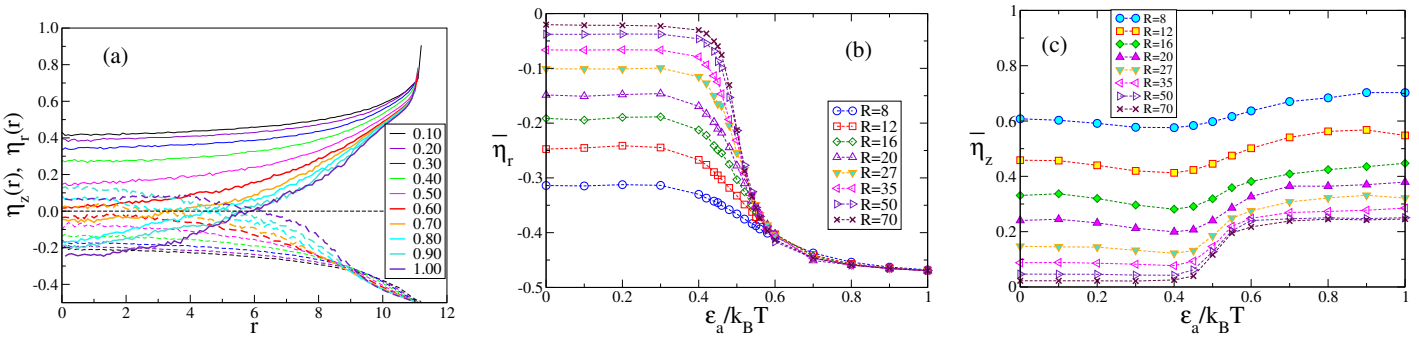


FIG. 5. (a) Spatially resolved orientational order parameters $\eta_z(r), \eta_r(r)$ (cf. Eqs.(9), (10)) plotted vs. $r$ for the case $R = 12$. Ten values of $\epsilon_a$ are included, as indicated in the legend. (b) Average order parameter $\bar{\eta}_r$, plotted as a function of the strength $\epsilon_a$ of the adsorption potential, for cylinder radii from $R = 8$ to $R = 70$, as indicated. Curves are guides to the eye only. (c) Same as (b) but for $\bar{\eta}_z$.

Thus, the finite size effects for this order parameter are similar to those for the adsorbed fraction $f$. We have also checked that finite size effects due to the finite chain length are similarly small as for $f$ by analyzing data for $\bar{\eta}_r$ for $N = 100$, 200 and 400 for $R = 20$ and $R = 35$. The order parameter $\bar{\eta}_z$, on the other hand, has a pronounced finite size behavior due to the finite magnitude of $R$ on both sides of the adsorption transition, Fig.5c. It converges to zero for $\epsilon < \epsilon_a^{cr}$ but it converges to 1/4 for $\epsilon_a > \epsilon_a^{cr}$. This happens because for $R \to \infty$ the bonds for $\epsilon_a > \epsilon_a^{cr}$ need not align in the $z$-direction but can take any direction parallel to the surface plane.

In the regime $\epsilon_a > \epsilon_a^{cr}$ the data for both $f$ and $\bar{\eta}_r$ indicate a rapid convergence towards nonzero order parameters in the limit $R \to \infty$. E.g., for $\epsilon_a = 0.7$ one finds from a corresponding extrapolation that there appears to be a convergence to $f = 0.884(5)$ and $\bar{\eta}_r = -0.446(1)$. However, the corresponding values for a planar wall were found to be systematically different, namely[78] $f = 0.994(1)$ and

$\bar{\eta}_r = -0,451(1)$, for the same choice of $\kappa = 25$ and $N = 200$. As a result, we conclude that the approach to the limiting behavior is a subtle problem when several of the characteristic lengths $R$, $L$ and $\ell_p$ are large and have a comparable magnitude.

### B. Chain linear dimensions

The delicate character of the approach of the properties of semiflexible polymer chains that are adsorbed on the wall of a cylindrical pore to the corresponding properties of the chains when they are adsorbed on a planar wall is clearly demonstrated when we study the total gyration radius square (Fig.6a) or the $z$-component of the root mean square end-to-end distance, Fig.6b. While initially these quantities decrease linearly as function of $1/R$ because for small $R$ the chains are very strongly stretched along the cylinder axis, for large $R$ they go through a minimum. Suppose an adsorbed chain at the cylinder surface would be oriented like a linear rigid rod: if it is oriented along the $z$-direction, no cost in bending energy arises while in tangential direction the chain can only be in a strongly adsorbed state, if it is systematically bent. Two subsequent bond vectors would need to form an angle $\gamma = \ell_b/R$, and hence a total bending energy cost of about $(N-1)\epsilon_a(\gamma^2)/2$ would arise. This bending energy becomes irrelevant, of course, when it is less than the thermal energy $k_BT$. So we predict a crossover for $R^*/\ell_b = \sqrt{\kappa N/2}$ which for $\kappa = 25$, $N = 200$, is about 50. Thus, only for $R \gg R^*$ the curvature of the cylindrical surface will be a small perturbation for the conformation of an adsorbed chain. Most of our data, however, were taken in the opposite regime, $R \ll R^*$, and in this regime a strong bias for the chain orientation in favor of the $z$-axis results. This minimum in the variation with $1/R$ is very pronounced for the gyration radius square, Fig.6a, but rather shallow for the $z$-component of the end-to-end distance, Fig.6b. In contrast, the variation of the $xy$-components, Fig.6c, is a monotonic increase with decreasing $1/R$, and this feature is responsible for the pronounced increase of the total gyration square as $1/R \to 0$.

As a consequence, we expect that the root mean square component of the end-to-end distance in $z$-direction is larger than in the tangential direction while on a planar surface both orientations are strictly equivalent. Hence we consider it as a surprise that at the cylinder surface the larger linear dimension of the adsorbed chain (in the $z$-direction) is smaller than the corresponding linear dimension on a planar surface for large $R$ (where $R$ exceeds $\ell_p$).

An interesting issue is also the behavior of the root mean square component of the end-to-end distance along the cylinder axis when it is studied as function of $\epsilon_a$ for $R < \ell_p$. We find that for $R = 8$ this quantity is almost independent of $\epsilon_a$, and very large, of order $0.81L$. For small enough $R$, when hairpin effects are completely negligible, precise theoretical predictions exist[35]

$$\frac{R_z}{L} = 1 - c_0 \left\langle \frac{2R}{\kappa} \right\rangle^{2/3} \tag{12}$$

which yields (using the result for $c_0 = 0.170$[35]) about $R_z/L = 0.8737$ for $R = 8$. So our data are only somewhat outside the regime where this theory asymptotically holds, given that $N = 200$ is not yet long enough so that hairpins could cause a significant reduction of $R_z$. This fact is expected, when one considers the prediction for the free energy cost of hairpin formation[35]

$$\frac{F}{k_BT} = C\frac{L}{\kappa} \left\langle \frac{\kappa}{2R} \right\rangle^{2/3}, \; C = 2.356 \tag{13}$$

which yields about 25.3 in our case. For larger $R$, the corresponding free energy would be smaller (e.g., 13.7 for $R = 20$), but still the $z$-component of the end-to-end distance is almost 50% of the contour length. For $R = 20$, we observe that $\langle R_{ez}^2 \rangle$ decreases first distinctly with increasing $\epsilon_a$,

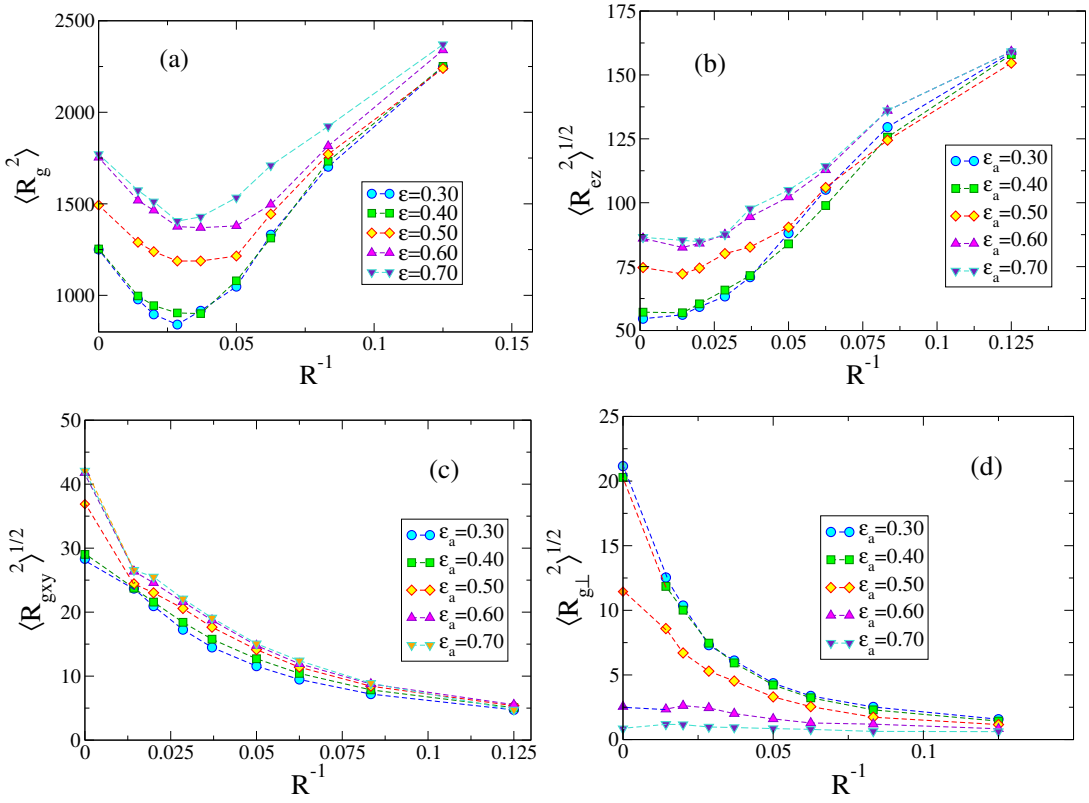


FIG. 6. $\langle R_g^2 \rangle$ (a), $\sqrt{\langle R_{ez}^2 \rangle}$ (b) , $\sqrt{\langle R_{gxy}^2 \rangle}$ (c), and $\sqrt{\langle R_{g,\perp} >^2 \rangle}$ (d) plotted versus $1/R$ for several choices of $\epsilon_a$, as indicated. The latter quantity denotes in (d) the component of $\langle Rg^2 \rangle$ perpendicular to the plane resulting from "unrolling" the cylindrical surface surrounding the chains.

reaching a minimum near $\epsilon_a = 0.3$ or $\epsilon_a = 0.4$, and then increases again. In this regime of $\epsilon_a$, the chain is neither strongly repelled nor strongly attracted by the surface, and so the full cylinder volume is actually available for the chain whereby the minimal extension in z-direction is understandable. For $R = 20$, the strongly adsorbed chain has a distinctly larger value (e.g., $\langle R_{ez}^2 \rangle = 12250$ for $\epsilon_a = 0.6$ rather than 7685 for $\epsilon_a = 0.3$). We interpret this strong increase in terms of the increase of the effective persistence length when the effective dimensionality changes from $d = 3$ to $d = 2$ due to adsorption, cf. Eq.(5).

While the MD simulation code uses the Cartesian coordinates $x$, $y$, $z$, there is not only interest in $x$, $y$-components of the radii of chains in cylinder geometry, of course. Even if the chains were strictly adsorbed on the wall and stretched out along the $z$-axis, due to averaging over the azimutal angle $\phi$ of the coordinates ($z$, $r$, $\phi$), transforming between Cartesian and cylindrical coordinates we always obtain $x$ , $y$ components of the radii of the order of $R$. In order to characterize the chain conformation in the cylinder, we are more interested in the radial distribution of the center of mass of the chains $\rho(r_{CM})$ and the components of the gyration radius of individual chains in radial direction. In order to better understand the chain conformations, we have found it useful to "unwrap" the cylinder surface into a plane ($X - Z$) and study the chain conformation in a Cartesian coordinate system where the radial direction then would always be the $Y$-component. Note that in this $X - Z$ plane there is a periodic boundary condition in $Z$-direction at $Z = H$, and in $X$-direction at $X = 2\pi R$. In the following,we use the subscripts "||" and "$\perp$" always referring to the "unrolled" plane $XZ$.

Fig.7 shows examples of chain configurations in such a coordinate system with an unrolled cylinder

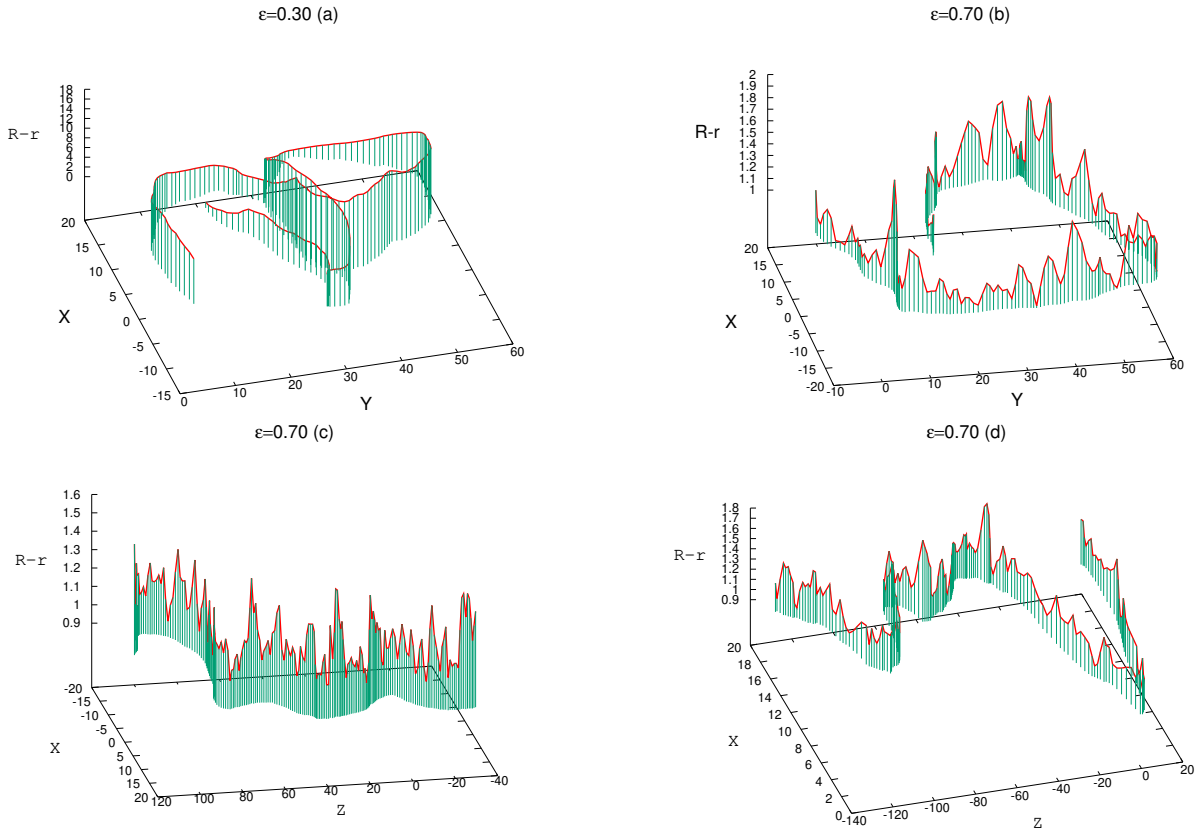


FIG. 7. Chain conformations for $R = 20$ relative to a cylinder surface unrolled into a plane with coordinates $X, Z$, with $Z$ along the cylinder axis $z$, and $X$ in tangential direction at a chosen point of the surface. The perpendicular coordinate $Y$ displays the radial distance to the surface $r' = R - r$ and is highlighted by the vertical straight green lines. Examples are for $\epsilon_a = 0.3$ (a) and 0.7 (b, c, d).

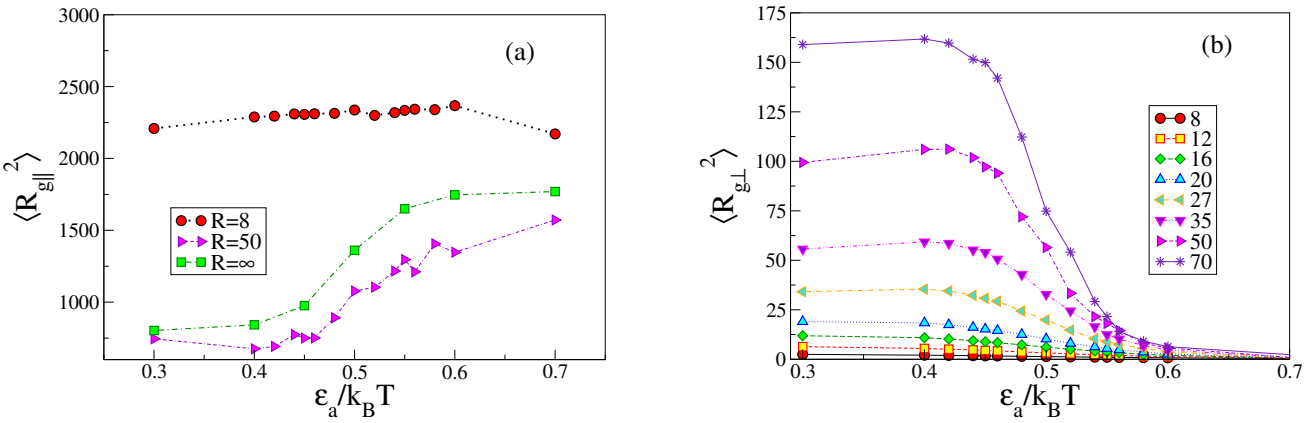


FIG. 8. $\langle R_{g||}^2 \rangle$ (a), and $\langle R_{g\perp}^2 \rangle$ (b) vs $\epsilon_a$ for pores with different radius $R$ as indicated. All data refer to the case $\kappa = 25$ and $N = 200$ throughout.

surface. Note the difference by an order of magnitude in the scale for $Y = r'$: for $\epsilon_a = 0.3$ hardly any monomers are close enough to the surface to be counted as adsorbed whereas almost all of them are adsorbed for $\epsilon_a = 0.7$. As in the planar case, the typical distance between the extrema of this curve describing the chain contour can be interpreted in terms of Odijk's deflection length concept[4], as discussed for the case of adsorption on a planar surface[77–79].

Already from the snapshot pictures it is plausible that the component of the gyration radius square

in the direction perpendicular to the confining surface is of order $R^2$ in the nonadsorbed case but only of order unity in the adsorbed case, as one can see more quantitatively in Fig.6d.

To summarize these results, Fig.8 shows the dependence of $\langle R^2_{g||} \rangle$ (a) and $\langle R^2_{g\perp} \rangle$ (b) on $\epsilon_a$: while the standard Cartesian components of either the end-to-end distance or gyration radius show hardly any direct effect of the adsorption transition of the polymer on the cylindrical wall, that shows up so clearly both in the snapshot pictures of the chains, Fig.1, and in the radial density distribution, both the parallel component $\langle R^2_{g||} \rangle$ and the transverse component $\langle R^2_{g\perp} \rangle$ of the "unwrapped" chains, parallel and perpendicular to the adsorbing surface that were illustrated in Fig. 7, manifest the signature of the adsorption transition very clearly.

### C. Distributions of train lengths, loop lengths, and tail lengths of the adsorbed chains

Traditionally[95], the conformation of adsorbed polymers is characterized by the concept of "trains, loops and tails" in the context of cubic lattice models where a polymer is described by a selfavoiding walk on the lattice, whereby only monomers (described then by occupied lattice sites) taken in the surface plane experience the energy gain due to adsorption. An uninterrupted sequence along the chain of such occupied lattice sites in the surface plane is called a "train" (irrespective of whether it runs all the way straight in a lattice direction or exhibits 90 degree kinks in the surface plane). "Loops" are portions of the chain which are connected to monomers which are in the surface plane, but all other monomers in the loop are further away from the surface. A linear polymer can have one or two "tails", with only one end of the sequence connected to a neighbor along the sequence that is in the surface plane. The number of monomers belonging to such sequences is denoted as the "length" of the train, loop, or tail, respectively.

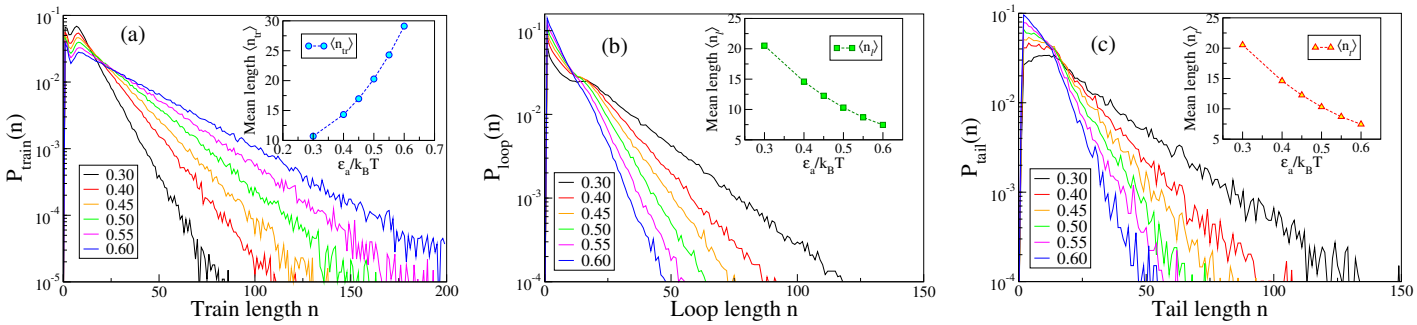


FIG. 9. (a) Distribution of train lengths plotted versus the train length on semi− log scales, for the case $N = 200$, $\kappa = 25$, and $R = 8$, including 6 choices of $\epsilon_a$, as shown in the legend. (b) Distribution of loop lengths versus the loop length, for the same case as panel (a). (c) Distribution of tail lengths versus the tail length, for the same case as panel (a). The mean lengths of trains $\langle n_{tr} \rangle$, loops $\langle n_l \rangle$, and tails $\langle n_t \rangle$, are plotted vs. $\epsilon_a$ in the shown inserts.

This concept can be carried over to off-lattice models as used here too, counting monomeric units which have a radial distance $r' < 2$ from the cylindrical surface as part of a train. Of course, for a smooth continuous adsorption potential this cutoff $r' = 2$ is somewhat arbitrary but we expect that the qualitative properties of the distributions of these lengths should not depend sensitively on the detailed choice of this cutoff.

Figs. 9 and 10 give two typical examples of these distributions, for the cases $R = 8$ and $R = 20$, respectively. We see that for large lengths $n$ of these trains, loops, or tails the data are compatible with a simple exponential decay for choices of $\epsilon_a$ where the chain is only partially adsorbed. An exception seems to be the case $R = 20$, $\epsilon_a = 0.6$, where $P_{train}(n)$ has a strong peak near $n = N$, and never large loops or long tails occur. Thus the curve for $P_{train}$ for $\epsilon_a = 0.6$ has been omitted

from Fig.10a. But from the study of the local order parameters we know already that this case is an example of a typically fully adsorbed chain. For small $n$, the distributions $P_{train}(n)$ exhibit a nonmonotonic variation with $n$ before the exponential decay starts to set in. Such a behavior was also seen for adsorption on planar surfaces[78], but a clear interpretation of this behavior is not obvious. Qualitatively, one might expect that a different behavior arises when $n < \lambda/\ell_b$ and when $n > \lambda/\ell_b$, $\lambda$ being the deflection length[4] which was also studied in[78]. But a full quantitative understanding of the values of this length for adsorbed chains is still lacking[78].

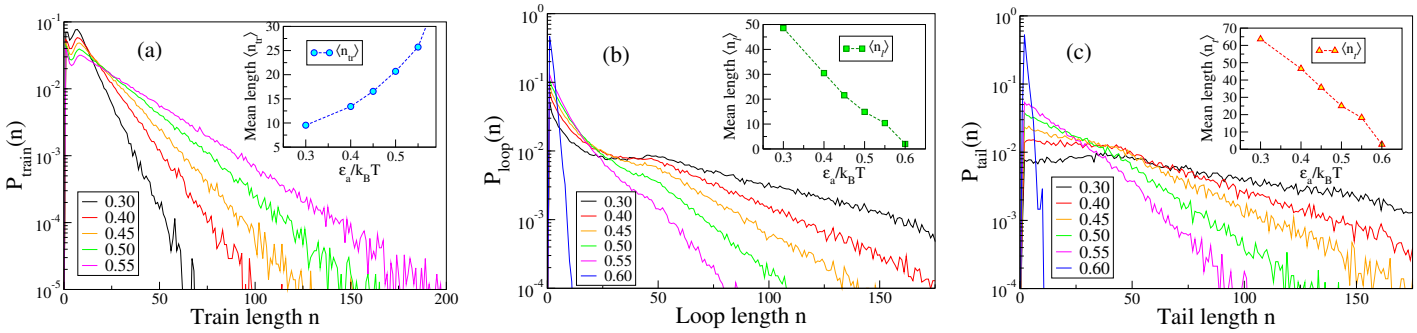


FIG. 10. (a) Same as Fig.9a, but for $R = 20$. (b) same as Fig.9b, but for $R = 20$. (c) same as Fig.9c, but for $R = 20$.

A special behavior is also seen in the loop length distribution, where for $\epsilon_a = 0.3$ a plateau at about $n = 25$ ($R = 8$) or $n$ between 25 and 50 ($R = 20$) occurs (Figs,9b, 10b). For planar walls[78], $P_{loop}(n)$ instead showed a smooth strongly nonexponential decay over a broad range of $n$. The detailed understanding of all these features is still a challenge.

The inserts in Figs.9 and 10 show the mean lengths of trains $\langle n_{tr}\rangle$, loops $\langle n_l\rangle$, and tails $\langle n_t\rangle$. The length $\langle n_{tr}\rangle$ increases with $\epsilon_a$ while the other two lengths decrease, as expected. We find that for smaller $R$ the average lengths are always systematically smaller, due to the finite size effects associated with the smallness of $R$. Note, however, that all these average lengths depend not only on $R$ and $\epsilon_a$, but a clear influence of the finite size of $N$ must also be expected when any of these average lengths is no longer very much smaller than $N$. However, a systematic study of these distributions for much larger values of $N$ would be very demanding in computer time resources, and hence has not been attempted.

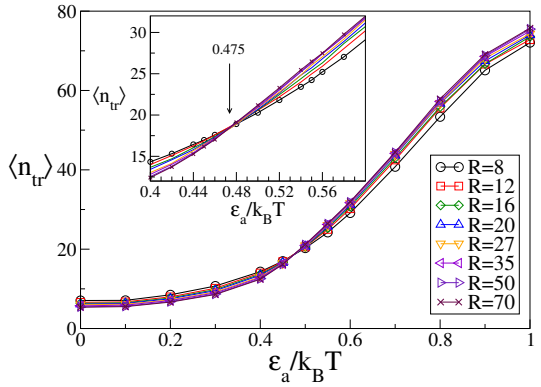


FIG. 11. Variation of the mean train length $\langle n_{tr}\rangle$ with strength of adsorption $\epsilon_a$ for cylinders with steadily growing radius $R$. The inset displays a magnified plot in the vicinity of the crossing point at $\epsilon_a^{cr}$ so as to emphasize the magnitude reversal with growing $R$.

An interesting finding is that the mean train length for $\epsilon_a < \epsilon_a^{cr}$ decreases with increasing $R$ but increases for $\epsilon_a > \epsilon_a^{cr}$, Fig.11. Indeed, for weak adsorption, $\epsilon_a < \epsilon_a^{cr}$, entropy drives the chains away

from the walls, therefore, the narrower the cylinder the larger is the fraction of monomers that still remain close to the walls, increasing thus effectively $\langle n_{tr} \rangle$. In contrast, for strong adsorption, $\epsilon_a > \epsilon_a^{cr}$, the attractive potential, Eq.(7), keeps the chains in the vicinity of the cylinder walls whereby the proximity of the surrounding cylindrical surface makes them intermittently attach to different parts of the narrow tube, decreasing thus effectively $\langle n_{tr} \rangle$. The intersection point estimate from Fig.11 is compatible with the estimate $\epsilon_a^{cr} = 0.48(1)$ for the planar wall[77–79] and may serve as an alternative method to determine $\epsilon_a^{cr}$ in cylindric confinement than the extrapolation, Fig.4c.

## IV. SUMMARY AND CONCLUSIONS

In this paper we study the competition between two types of conformational changes of isolated semiflexible polymer chains under good solvent conditions, namely, the confinement inside a long cylindrical pore with cylinder radius $R$, and the adsorption on the cylindrical surface of this pore, triggered by a potential (Eq.7) whose strength $\epsilon_a$ is a second control parameter. We use Molecular Dynamics simulation methods and apply a coarse-grained bead-spring type model (Eqs.1-3) which has essentially 3 parameters: the effective chain diameter $\sigma$ which is our length unit, the chain stiffness $\kappa$, and the chain length $N$ (i.e., the number of effective monomeric units along the chain; the distance between these units along the backbone of the chain is of order $\sigma$ as well).

If one has the application to ds-DNA in mind, $\sigma$ would physically correspond to $2\,nm$ and $\kappa = 25$ then corresponds to the typical value of the persistence length of $50\,nm$; however, we do not attempt a more realistic modeling which would require to consider electrostatic interactions, of course. Our model qualitatively would correspond to the limit where the electrostatic interactions are strongly screened. Thus, also our adsorption potential (Eq.7) is of the van der Waals type only. Being interested in the behavior of long chains, we focus on the choice $N = 200$. However, for the adsorption on planar walls there is a strong finite-size-effect due to this finiteness of $N$, and a comparative study of several choices of $N$ over a broad range of chain lengths is indispensable to characterize the adsorption behavior. Yet, for the present choices of $R$ (from $R = 8$ to $R = 70$) the finite size rounding of the adsorption transition caused by the finiteness of $R$ rules the behavior still almost exclusively.

This strong finite-size rounding of the adsorption transition in the cylindrical pore (truly singular behavior associated with this transition occurs only when both the limits $N$ to infinity and $R$ to infinity are taken) shows up both in the local "order parameters" of the adsorption transition, such as the adsorbed fraction of monomeric units $f$ and the bond orientational order parameter $\bar{\eta}_r$, (Figs.4a, 5b) when the strength of the adsorption potential $\epsilon_a$ is varied. The rounding shows up in the chain linear dimensions as well, Fig.6. For a study of this behavior, $N = 200$ turned out to be long enough as a test using other chain lengths ($N = 100$ and $N = 400$) showed.

When we vary the strength of the adsorption potential, three regimes can be distinguished, at least qualitatively: for small $\epsilon_a$, the chain avoids the region close to the cylindrical surface, due to entropic repulsion the local monomers density decreases in the region $\sigma \ll r' = R - r \ll R \propto (r'/R)^2$, while for $r' < \sigma$ due to enthalpic repulsion the density is almost completely suppressed. Due to the monomeric units that still occur in the region from $r' = \sigma$ to $r' = 2\sigma$ a "finite size tail"[80] of order $1/R^2$ arises. Also the orientational order parameter (Fig.4b) shows a similar behavior. For small $R$, the chain extension along the pore $\langle R_{gz}^2 \rangle$ decreases in this region slightly with increasing $\epsilon_a$, as a more uniform density distribution inside the pore is reached (e.g., for $\epsilon_a$ in the range between 0.3 and 0.4) before it increases again due to adsorption. Thus, $\langle R_{gz}^2 \rangle$ as function of $\epsilon_a$ exhibits a shallow minimum. A similar phenomenon was detected for fully flexible polymers already in an early work[11]. In this regime of $\epsilon_a$ also a crossover of the power law for the decay of $f$ and $\bar{\eta}_r$ with $R$ from $1/R^2$

to a much slower decay is found, namely roughly $f_c \propto 1/R^{1/3}$ (Fig.4b). Also a finite-size shift of the "effective" adsorption transition point (defined from the inflection point of the $f$ vs. $\epsilon_a$ or $\bar{\eta}_r$ vs. $\epsilon_a$ curves) is found, namely $\epsilon_a^{cr}$ - $\epsilon_a^{infl} \propto 1/R$ (Fig.4c).

A very interesting nonmonotonic behavior of the total mean square gyration radius and the $z$-component with $1/R$ is also found, Fig.6a,b. For small enough $R$, the chains are strongly stretched along the cylinder axis (reaching an end-to-end distance of the order of the contour length for $R < 8$). For $R$ of the order of the persistence length, a shallow minimum is reached, followed by an increase linear in $1/R$ as $1/R \to 0$. The large values for adsorbed chains on planar surfaces (reached for $1/R = 0$) reflect the fact that a doubling of the persistence length and hence of the squared gyration radii occurs when one goes from $d = 3$ to $d = 2$ dimensions. For finite $R$ and rather strongly adsorbed chains, there clearly is a conflict between the curvature of the attracting substrate (which would favor slightly bent sections of the chain having the length $\ell_p$ and banana-like shape) and chain stiffness $\kappa$ of our model (which favors on average a straight conformation over the scale of the persistence length). On the other hand, when we consider $\langle R_{gxy}^2 \rangle$ and $\langle R_{g\perp}^2 \rangle$, we find a monotonous variation with $1/R$. Recall that for our choice of coordinate system, with the $z$-axis being the cylinder axis, $\langle R_{gz}^2 \rangle$ converges (essentially) to 1/2 of the parallel component of a strongly adsorbed chain on a planar substrate, since for the planar substrate $x$- and $z$-directions are equivalent, and $y$ in the limit $1/R \to 0$ is orthogonal to the plane.

It is remarkable that the chain actual linear dimensions in the cylinder, e.g., $\langle R_g^2 \rangle$, $\langle R_{ez}^2 \rangle$, $\langle R_{gxy}^2 \rangle$, when one studies them as function of $\epsilon_a$, are affected very weakly by the adsorption on the cylindrical wall, unlike the behavior that one finds for adsorption on a planar wall. The components $\langle R_{g||}^2 \rangle$ and $\langle R_{g,\perp}^2 \rangle$ of the "unwrapped conformation", Fig.8, (parallel and perpendicular to the cylinder surface that is then "unrolled " into a planar surface) show clear signatures of the adsorption transition.

It is also demonstrated that the cylindrical confinement causes a remarkable local stiffening of the wormlike chains which is evident from the study of an effective persistence length related to $\langle \cos(\theta) \rangle$, where $\theta$ is the angle between subsequent bond vectors along a chain (Fig.1).

We have also analyzed the distributions of the lengths of trains, loops and tails in the vicinity of the adsorption transition, Figs.9-11. Particularly interesting is the distribution of trains lengths $\langle n_{tr} \rangle$, which for large $\langle n_{tr} \rangle$ exhibits an exponential decay both below the adsorption threshold and slightly above it as well (Figs.9a, 10a). But the transition itself shows up clearly as a crossing point at $\epsilon_a^{cr}$ in the plot of $\langle n_{tr} \rangle$ vs. $\epsilon_a$ for different $R$ (Fig.11).

We hope that our study helps to understand experiments that address the adsorption behavior of semiflexible polymers in various types of cylindrical confinement. As a caveat, however, we mention that in experiments adsorption of polymers often needs to be treated as an irreversible process[96,97], leading to distributions of loops, tails and trains that differ from those observed in full thermal equilibrium.

## ACKNOWLEDGMENTS

One of us (A.M.) is grateful to the Alexander-von-Humboldt foundation for financial support and also thanks the COST action No. CA17139, supported by COST (European Cooperation in Science and Technology [See http://www.cost.eu and https://www.fni.bg] and its Bulgarian partner FNI/MON under KOST-11

## References

[1] E. F. Casassa, J. Polym. Sci. B **5**, 773 (1967).
[2] E. F. Casassa and Y. Tagami, Macromolecules **2**, 14 (1969).
[3] M. Daoud and P. G. de Gennes, J. Phys. (Paris) **38**, 85 (1977).
[4] T. Odijk, Macromolecules **16**, 1340 (1983).
[5] K. Kremer and K. Binder, J. Chem. Phys. **81**, 6381 (1984).
[6] W. Helfrich and W. Harbich, Chem. Scr. **25**, 32 (1985).
[7] T. Odijk, Macromolecules **19**, 2313 (1986).
[8] M. G. Davidson, U. W. Suter, and W. M. Deen, Macromolecules **20**, 1141 (1987).
[9] E. Raphael and P. Pincus, J. Phys. (France) II **2**, 1341 (1992).
[10] M. Dijkstra, D. Frenkel, , and H. N. W. Lekkerkerker, Physica A **193**, 374 (1993).
[11] A. Milchev, W.Paul, and K.Binder, Macromol. Theory and Simul. **3**, 305 (1994).
[12] A. Gorbunov and A. M. Skvortsov, Adv. Colloid Interface Sci. **62**, 31 (1995).
[13] G.M.Guttman, E. A. DiMarzio, and J. F. Douglas, Macromolecules **29**, 5723 (1996).
[14] T. W. Burkhardt, J. Phys. A: Math. Gen. **30**, L167 (1997).
[15] A. M. Skvortsov, A. A. Gorbunov, D. Berek, and B. Trathnigg, Polymer **39**, 423 (1998).
[16] T. W. Burkhadrt and I. Guim, Phys. Rev. E **59**, 5833 (1999).
[17] P. Cifra and T. Bleha, Polymer **41**, 1003 (2000).
[18] Y. Gong and Y. Wang, Macromolecules **35**, 7492 (2002).
[19] B. Morrison and D. Thirumalai, J. Chem. Phys. **122**, 194907 (2005).
[20] W. Reisner, K. J. Morton, R. Riehn, Y. M. Wang, Z. Yu, M. Rosen, J. C. Sturm, S. Y. Chou, E. Frey, and R.H.Austin, Phys. Rev. Lett. **94**, 196101 (2005).
[21] J. Wang and H. Gao, J. Chem. Phys. **123**, 084906 (2005).
[22] F. Brochard-Wyart, T. Tanaka, N. Borghi, and P. G. de Gennes, Langmuir **21**, 4144 (2005).
[23] T. Sakaue and E. Raphael, Macromolecules **39**, 2621 (2006).
[24] K. Avramova and A. Milchev, J. Chem. Phys. **124**, 024909 (2006).
[25] T. Odijk, J. Chem. Phys. **125**, 204904 (2006).
[26] A. Arnold, B. Bozorgui, and D. Frenkel, J. Chem. Phys. **127**, 164903 (2007).
[27] Y. Yang, T. W. Burkhardt, and G. Gompper, Phys. Rev. E **76**, 011804 (2007).
[28] F. Valle, M. Favre, P. D. L. Rios, A. Rosa, and G. Dietler, Phys. Rev. Lett. **95**, 158105 (2007).
[29] T. Odijk, Phys. Rev. E **77**, 060901(R) (2008).
[30] G. Morrison and D.Thirumalai, Phys. Rev. E **79**, 011924 (2009).
[31] Y. Wang, D. R. Tree, and K. D. Dorfman, Macromolecules **44**, 6594 (2011).
[32] P. Cifra, J. Chem. Phys. **136**, 024902 (2012).
[33] W.Reisner, J. N. Pedersen, and R. H. Austin, Rep. Prog. Phys. **75**, 106601 (2012).
[34] D. R. Tree, Y. Wang, and K. D. Dorfman, Phys. Rev. Lett. **110**, 208103 (2013).
[35] J. Z. Y. Chen, Macromolecules **46**, 9837 (2013).
[36] L. Dai and P. S. Doyle, Macromolecules **46**, 6336 (2013).
[37] A. Muralidhar, D. R. Tree, Y. Wamg, and K. D. Dorfman, J. Chem. Phys. **140**, 084905 (2014).
[38] L. Dai, J. van der Maarel, and P. S. Doyle, Macromolecules **47**, 2445 (2014).
[39] A. Murahlidhar, D. R. Tree, and K. D. Dorfman, Macromolecules **47**, 8446 (2014).
[40] K. D. Dorfman, D. Gupta, A. Jain, A. Muralidhar, and D. R. Tree, Eur. Phys. J. Special Topics **223**, 3179 (2014).
[41] E. Werner and B. Mehlig, Phys. Rev. E **91**, 050601(R) (2015).
[42] A. Muralidhar, M. J. Quevillon, and K.D.Dorfman, Polymers **8**, 79 (2016).
[43] J. Z. Y. Chen, Progr. Polym. Sci. **54-55**, 3 (2016).

[44] J. Z. Y. Chen, Phys. Rev. Lett. **118**, 247802 (2017).
[45] E.Werner, A. Jain, A. Muradhilar, K. Frijkholm, T. S. C. Smithe, J. Fritzsche, F. Westerlund, K. D. Dorfman, and B. Mehlig, Biomicrofluidics **12**, 024105 (2018).
[46] S. Bernier, S. Huang, W. Reisne, and A. Bhattacharya, Macromolecules **51**, 4012 (2018).
[47] A. Milchev and K. Binder, Soft Matter **17**, 3443 (2021).
[48] S. J. Gregg and K. S. W. Sing, Ber. Bunsenges. Phys. Chem. **86**, 957 (1982).
[49] S. Lowell, J. E. Shields, M. A. Thomas, and M. Thommes, *Characterization of Porous Solids and Powders. Surface Area, Pore Size, and Density* (Springer, Berlin, 2012).
[50] J. Rouquerol, F. Rouquerol, P. Llewellin, G. Mourin, and K. S. W. Sing, *Adsorption by Powders and Porous Solids. Principles, Methodology, and Applications* (Academic Press, New York, 2013).
[51] M. Muthukumar, C. Plesa, and C. Debber, Phys. Today **68**, 40 (2015).
[52] C. Y. Kong and M. Muthukumar, Electrophoresis **23**, 2697 (2002).
[53] M. Muthukumar, *Polymer Translocation* (CRC Press, Boca Raton, 2011).
[54] A. M. M. Jani, D. Losic, and N. H. Voelcker, Progr. Mat. Sci. **58**, 636 (2013).
[55] K. V. Kumar, K. Preuss, M. M. Titirici, and F. Rodriguez-Reinisi, Chem. Rev. **117**, 1796 (2017).
[56] T. Hofmann, *Soft Matter under Confinement*, edited by P. Huber (World Scientific, Singapore, 2020) p. 435.
[57] P. G. de Gennes, *Scaling Concepts in Polymer Physics* (Cornell Universit Press, Ithaca, N. Y, 1979).
[58] A. Grosberg and A. R. Khokhlov, *Statistical Physics of Macromolecules* (AIP Press, New York, 1994).
[59] M. Rubinstein and R. Colby, *Polymer Physics* (Oxford University Press, New York, 2003).
[60] H.-P. Hsu, W. Paul, and K. Binder, Macromolecules **43**, 3094 (2010).
[61] O. Kratky and G. Porod, J. Colloid Sci. **4**, 35 (1949).
[62] H. Nakanishi, J. Phys. (Paris) **48**, 979 (1987).
[63] J. Moon and H. Nakanishi, Phys. Rev. A **44**, 6427 (1991).
[64] H.-P. Hsu, W. Paul, and K. Binder, Europhys. Lett. **92**, 28003 (2010).
[65] H. Pasch, C. Brinkmann, H. Much, and U. Just, Chromatogr. **623**, 315 (1992).
[66] D. Berek, M. Janćo, and G. Meira, J. Polym. Sci. A **36**, 1369 (1998).
[67] M. J. andT. Hirano, T. Kitayama, K. Hatada, and D. Berek, Macromolecules **33**, 1710–1715 (2000).
[68] J. Falkenhagen, H. Much, W. Stauff, and A. H. E. Mueller, Macromolecules **33**, 3687 (2000).
[69] W. Lee, H. Lee, H. C. Lee, D.Choo, T. Chang, A. A. Gorbunov, and J. Roovers, Macromolecules **35**, 529 (2002).
[70] R. Sinha, H. L. Frisch, and F. R. Eirich, J. Chem. Phys. **57**, 584 (1953).
[71] E. Eisenriegler, *Polymers Near Surfaces* (World Scientific, Singapore, 1993).
[72] P. Grassberger, J. Phys. A: Math. Gen. **38**, 323 (2005).
[73] L. I. Klushin, A. A. Polotsky, H.-P. Hsu, D. A. Markelov, K. Binder, and A. M. Skvortsov, Phys. Rev. E **87**, 022604 (2013).
[74] T. M. Birshtein, E. B. Zhulina, and A. M. Skvortsov, Biopolymers **18**, 1171 (1979).
[75] A. N. Semenov, Eur. Phys. J. E **9**, 353 (2002).
[76] M. Deng, Y. Jiang, H. Liang, and J. Z. Y. Chen, J. Chem. Phys. **133**, 034902 (2010).
[77] A. Milchev and K. Binder, Phys. Rev. Lett. **123**, 128003 (2019).
[78] A. Milchev and K. Binder, Polymers **12**, 255 (2020).
[79] A. Milchev and K. Binder, J. Chem. Phys. **152**, 064901 (2020).
[80] V. P. (ed.), *Finite Size Scaling and Numerical Simulation of Statistical Systems* (World Scientific,

Singapore, 1990).
[81] T. A. Kampmann, H.-H. Boltz, and J. Kierfeld, J. Chem. Phys. **139**, 034903 (2013).
[82] M. L. Sushko, A. L. Shluger, and C. Rivetti, Langmuir **22**, 7678 (2006).
[83] C. R. Safinya, I. Koltover, and J. Raedler, Current Opin. Colloid Interface Sci. **3**, 69 (1998).
[84] P. Huber, S. Grüner, C. Schäfer, K. Knorr, and A. V. Kityk, Eur. Phys. J. Special Topics **141**, 101–105 (2007).
[85] S. J. de Cavalho, R. Metzler, and A. G. Cherstvy, Soft Matter **15**, 4430 (2015).
[86] S. A. Egorov, A. Milchev, and K. Binder, Phys. Rev. Lett. **116**, 187801 (2016).
[87] J. D. W. D. Chandler and H. C. Andersen, J. Chem. Phys. **54**, 5237 (1971).
[88] G. S. Grest and K. Kremer, Phys. Rev. A **33**, 3628(R) (1986).
[89] K. Binder, ed., *Monte Carlo and Molecular Dynamics Simulations in Polymer Science* (Oxford University Press, New York, 1995).
[90] L. Schäfer, A. Ostendorf, and J. Hager, J. Phys. A: Math. Gen. **32**, 7875 (1999).
[91] X. Xu, G. Vereecke, C. Chen, G. Pourtois, S. Armini†, N. Verellen, W.-K. Tsai, D.-W. Kim, E. Lee, C.-Y. Lin, P. V. Dorpe, H. Struyf†, F. Holsteyns†, V. Moshchalkov, J. Indekeu, and S. D. Gendt†, ACS Nano **8**, 885 (2014).
[92] S. Matysiak, A. Montesi, M. Pasquali, A. B. Kolomeisky, and C. Clementi, Phys. Rev. Lett. **96**, 118103 (2006).
[93] L. Andersen, C. Lorenz, and J. Travesset, J. Comput. Phys. **227**, 5342 (2008).
[94] J. Glaser, T. D. Nguyen, J. A. Anderson, P. Lui, F. Spiga, J. A. andD. C. Morse, and S. C. Glotzer, J. Comput. Phys. **192**, 97 (2015).
[95] C. J. Fleer, M. A. Cohen-Stuart, J. M. H. Scheutjens, T. Cosgrove, and B. Vincent, *Polymers at Interfaces* (Chapman & Hall, London, 1993).
[96] N.-K. Lee, Y. Jung, and A. Johner, Macromolecules **48**, 7681 (2015).
[97] Y. Kim, M.-K. Chae, N.-K. Lee, Y. Jung, and A. Johner, Macromolecules **50**, 6285 (2017).

TOC graphics